Advancing Volumetric Additive Manufacturing via Radio Frequency Energy Delivery: Process Development & Characterization

by

Matthew L. McCoy

Submitted to the George W. Woodruff School of Mechanical Engineering
in partial fulfillment of the requirements for the degree of

DOCTOR OF PHILOSOPHY IN MECHANICAL ENGINEERING

at the

GEORGIA INSTITUTE OF TECHNOLOGY

Authored by: Matthew L. McCoy
Ph.D. Student
George W. Woodruff School of Mechanical Engineering

Advised by: Carolyn C. Seepersad, Ph.D.
Professor of Mechanical Engineering
Woodruff Professor, Thesis Supervisor

Advised by: Christopher J. Saldaña, Ph.D.
Professor of Mechanical Engineering
Ring Family Professor, Thesis Supervisor

Contents

Introduction

Additive manufacturing (AM) has revolutionized fabrication by enabling complex geometries, rapid prototyping, and distributed production through increasingly accessible machines and materials [1–8]. Among powder bed fusion (PBF) techniques, Selective Laser Sintering (SLS) remains widely adopted for polymer AM due to its geometric flexibility and robust mechanical performance [9–11].

However, SLS presents considerable limitations. The process is inherently inefficient: only a small fraction of the thermal energy directly contributes to part formation, while the majority heats unused surrounding powder [11, 12]. Prolonged exposure of the powder to high temperatures also degrades polymers such as PA12, commonly known as Nylon 12, which can only withstand approximately 5–7 thermal cycles before exhibiting reduced mechanical strength, ductility, and reliability [13–20]. Maintaining a uniformly elevated build chamber temperature further amplifies energy losses, while creating inconsistent thermal gradients that drive residual stresses and warping [10, 21]. These thermal side effects also lead to powder caking and semi-sintered boundaries, increasing post-processing effort [11].

Production throughput is similarly constrained. Build rates in SLS are limited by the time required to expose every voxel with a scanned laser. Increasing speed requires either higher laser power or multiple lasers, both of which introduce practical limitations. Excessive energy density risks material degradation or ablation unless scan speed is increased, but this is constrained by galvanometer performance. While adding lasers can increase throughput, it also raises system cost and complexity significantly [10, 21, 22].

These limitations are not only technical, but they carry significant economic penalties. Machine depreciation dominates part cost in SLS, not raw materials or tooling [23, 24]. Capital equipment often exceeds $250,000[1], yet builds are slow, producing as few as ten parts per week [25, 27]. To recover capital investment over a typical five-year lifespan, each part must carry a significant cost burden from machine depreciation alone, which is often over $100 per part [23]. Consequently, increasing build rate is not merely about saving time, but about reducing part cost. Faster, more efficient build processes are needed, and *Radio Frequency Additive Manufacturing (RFAM)* offers a fundamentally different approach.

By volumetrically coupling radio frequency energy into doped regions of the powder bed, RFAM selectively melts targeted areas without meaningfully raising the temperature of surrounding material [28–30]. In RFAM, a dopant such as carbon black is selectively deposited onto the powder bed in a layer-by-layer fashion using an inkjet printhead, after which the resulting green (or brown) part is extracted and exposed to radio frequency energy for sintering. This process decouples energy input from surface scanning, enabling higher throughput, minimizing thermal waste, and reducing the number of thermally cycled powder particles, illustrated in Figure 1. Additionally, volumetric heating holds promise for improved material homogeneity and reduced residual stress by eliminating interlayer reheating [13, 31].

The absence of heat in non-targeted regions minimizes sintered artifacts in surrounding powder, reducing post-processing effort [10]. The RFAM platform also avoids reliance on precision scanning optics, allowing for scalable designs without major system complexity.

[1]Multiple sources report PBF system prices exceeding $250,000, including Khajavi et al. [25] and Barclift et al. [26].

This volumetric and targeted approach positions RFAM as a novel next-generation AM technology, offering higher production rates, improved material and energy efficiency, and lower total cost of ownership.

Despite its potential to overcome many of the limitations inherent to Selective Laser Sintering, Radio Frequency Additive Manufacturing remains in its early stages. Significant questions remain regarding process control, achievable precision, and the adaptability of the technique to a broader range of materials beyond standard polymer/dopant systems [30]. This work seeks to address these open questions by advancing RFAM process control, simulation, and material expansion.

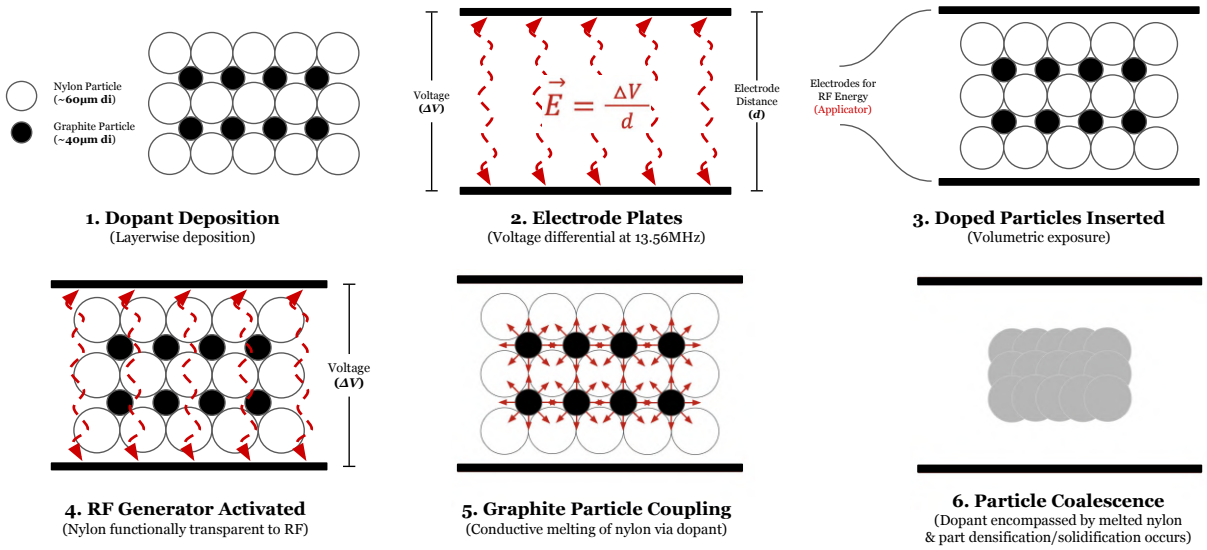

Figure 1: Illustration of the RFAM sintering mechanism. Carbon/graphite-doped nylon powder is exposed to an RF field between copper electrode plates. The dopant selectively absorbs RF energy, generating heat that melts the surrounding nylon, enabling particle coalescence and part densification.

This dissertation investigates RFAM as a platform for next-generation, energy-efficient, and high-throughput polymer additive manufacturing, with a focus on the underlying mechanisms of volumetric sintering, system design constraints, and predictive modeling. By combining experimental, computational, and systems-level approaches, this work aims to address the fundamental challenges of RFAM and evaluate its viability as an emerging AM technology.

0.1 Research Objectives

This work is organized around three core tasks:

1. **Design and Characterization of a Custom RFAM Platform:** A custom binder jet-style machine is designed and built to enable comprehensive exploration of the RFAM process. This platform serves as the experimental foundation for all process development and characterization efforts. To evaluate deposition performance, a framework is established for quantifying jetting fidelity and dopant control. These methods enable high-resolution measurement of key metrics without reliance on high-end instrumentation. The resulting data inform a model that (1) classifies ink concentration levels and (2) evaluates dimensional accuracy while compensating for a range of system-level mechanical errors. Together, these approaches provide a practical, machine-agnostic means of validating system performance and guiding error correction in RFAM.

2. **Toward Ideal Parts and Geometric Precision via Computational Solutions:** Advanced computational methods and multiphysics finite element analysis (FEA) are employed to simulate the RF heating process. These models capture the interplay between electromagnetic fields, thermal diffusion, and sintering kinetics, in the effort of optimizing dopant distributions to achieve uniform temperature profiles. Computational strategies such as functional grading and pre-distortion are applied to improve control over spatial energy absorption. The resulting simulations inform solutions to key RFAM challenges, including shrinkage management, void suppression, boundary control, and field uniformity. To support these efforts, custom inks are formulated to enable high dopant concentrations.

3. **Expansion of Material Systems and Process Modalities:** RFAM is extended beyond conventional nylon/carbon-black systems by introducing new materials, dopants, and RF activation strategies. These efforts include investigating RF-curable silicones for extrusion-based bath printing, RF-induced foam expansion in silicone composites, and selectively actuated geometries responsive to RF exposure. The objective is to demonstrate RFAM's adaptability to novel material classes and non-powder-bed platforms, advancing it toward a general-purpose energy-mediated manufacturing paradigm.

Through system design, fabrication, and characterization, coupled with simulation-driven process control and the introduction of novel material systems and process modalities, this research advances RFAM toward improved process fidelity, enhanced part quality, and broader technological applicability.

Task 1: Design and Characterization of a Custom Radio Frequency Additive Manufacturing Platform

This task presents the design, implementation, and validation of a custom Radio Frequency Additive Manufacturing (RFAM) platform developed to explore volumetric sintering through patterned dopant deposition and targeted RF energy delivery.

1.1 Design of a Modular RFAM Platform

The successful implementation of RFAM requires a custom-built machine architecture capable of precise powder handling, dopant patterning, controlled heating, and electromagnetic isolation. To this end, a modular RFAM platform was designed and constructed, integrating industrial automation hardware with custom-fabricated components to support high-resolution experimentation. The system includes four major subsystems: an external RF energy delivery system, a material handling unit, printhead gantry, and recoater & evaporation gantry (Figures 1.1 & 1.2).

The motion platform features high-precision ball screw actuators for gantry motion and enclosed belt drives for vertical piston movement. The hardware was selected for its modularity and rapid deployment timeline, enabling a functional motion platform to be delivered within four months of project initiation. This platform supports the mounting of all critical systems and has demonstrated sub-100 µm repeatability, forming the mechanical backbone of the RFAM process.

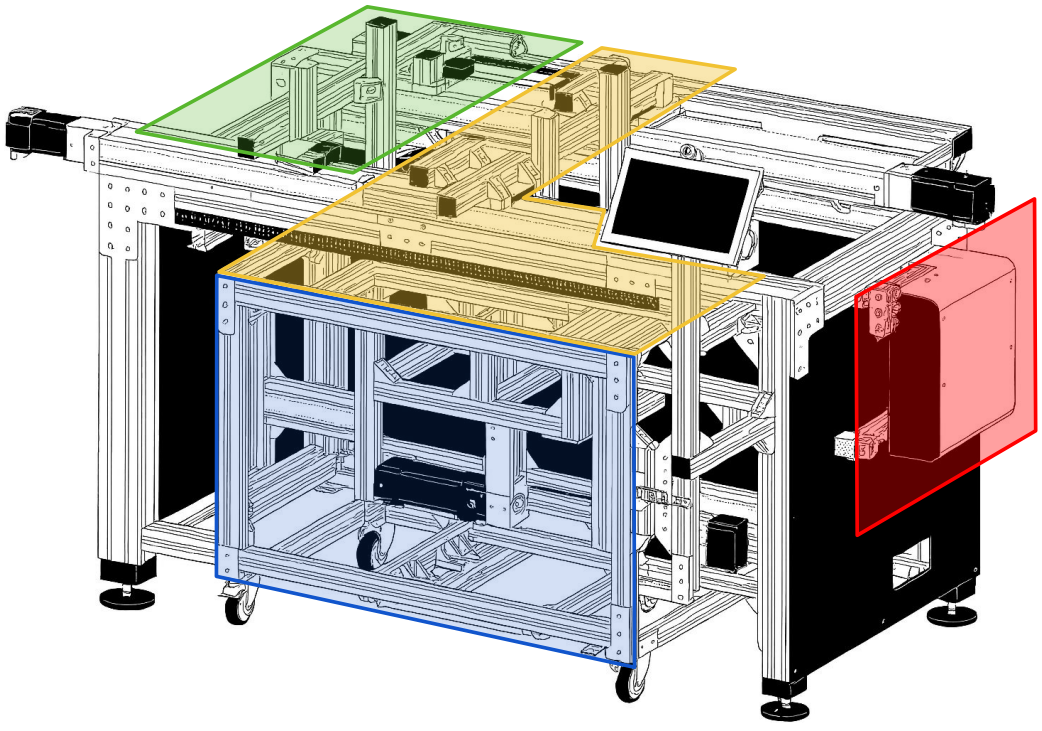

Figure 1.1: Drawing of custom RFAM binderjet–style platform showing a removable material-handling unit (blue), a printhead gantry (green), a recoating/evaporation gantry (yellow), and motor control unit (red).

Material Handling: The material handling subsystem includes two cylindrical build chambers, consisting of a feed cylinder and a part cylinder, mounted on a removable cart that interfaces with the printer through a rail-guided ingress/egress mechanism. The cylinders and pistons are made from RF-transparent materials (e.g., PLA or nylon) to prevent further field distortion during energy delivery. A compliant sealing ring system was developed using printed spring geometries to maintain powder containment without metal components, which would interfere with RF coupling.

Printhead Gantry: The dopant patterning subsystem employs Xaar Aquinox 2002 printheads capable of jetting high-viscosity inks (50+ cP) with particle loadings up to 50 wt% [32]. These heads are mounted to a machined aluminum printbar supported by an adjustable mounting plate and linear Z-stage. The mount enables fine-tuning of printhead parallelism relative to the powder bed and supports dynamic calibration across multiple experimental setups. Ink system components are mounted on a rear panel to facilitate maintenance and minimize tubing lengths.

Recoater & Evaporation Gantry: A machined aluminum blade recoater is mounted to a second gantry for uniform layer spreading. The blade angle and height are independently adjustable using spring-loaded leveling mounts, allowing for precision alignment relative to the printing substrate. A dial indicator mount is integrated onto the recoater assembly to support substrate tramming and ensure planarity between motion axes and the powder surface. A 500 W quartz tube heater, described below, is also mounted to this assembly.

RF Energy Delivery: Following dopant deposition, the solvent base of the printed ink must be removed before sintering. A 500 W quartz tube heater, mounted on the recoater gantry, is used to drive solvent evaporation. After printing, the part cylinder is transferred to an RF sintering station. This station integrates: a 600 W, 13.56 MHz RF generator (AG0613) and an AIT-600 automatic impedance matching network, both from T&C Power Conversion, Inc.; a Faraday cage (RF leakage attenuation) with parallel copper electrodes; and a motorized turntable that rotates the part to ensure isotropic field exposure.

Together, these subsystems form a robust and configurable RFAM research platform, supporting high-resolution dopant patterning, process control experimentation, and integration with ex-situ diagnostics.

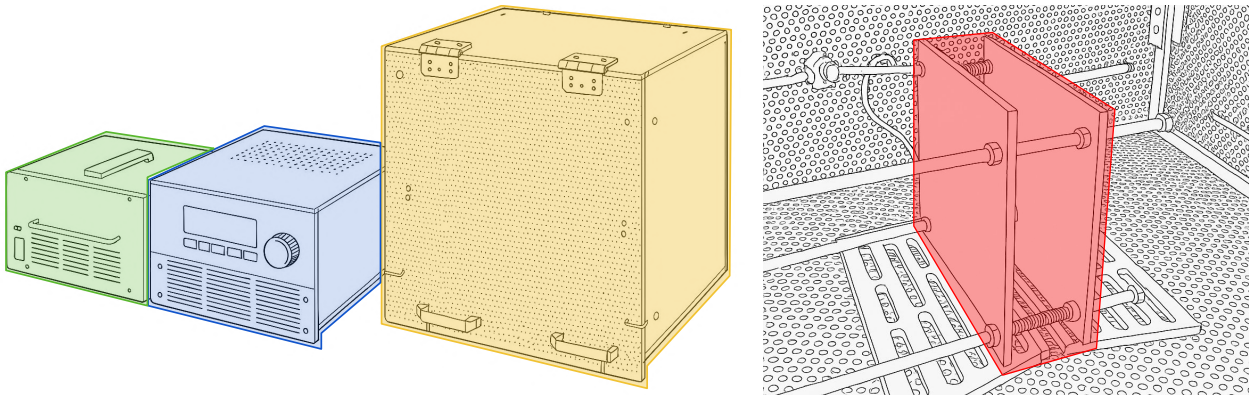

Figure 1.2: Illustration of the RF energy delivery system: RF impedance matching network (green), 600 W, 13.56 MHz RF generator (blue), Faraday cage (yellow), and electrodes (red).

1.2 Development of a Low-Cost, Ex-Situ Diagnostic Tool

Print quality metrics, such as granularity, banding, and positional inaccuracy, are widely studied in conventional and digital printing. These are often measured using flatbed scanners or digital cameras [33, 34]. In inkjet-printed electronics and paper-based analytical devices, image-based metrology and quantitative color analysis are increasingly standard [35–38]. More advanced metrology approaches, such as digital image correlation (DIC) and confocal microscopy, offer higher resolution but are often impractical for rapid or routine diagnostics [38].

Recent studies have applied machine learning and computer vision to diagnose printing defects and predict failure modes using 2D image data [34, 39]. These developments highlight the growing importance of robust, quantitative diagnostic tools in both academic and industrial additive manufacturing workflows.

To complement modeling and provide an experimental foundation, this work introduces a scanner-based diagnostic pipeline for evaluating jetting fidelity and dopant distribution in the RFAM platform. The method uses high-resolution flatbed scanners alongside both low-wicking and absorptive paper substrates to produce quantitative data on spatial placement and optical density, respectively. The diagnostic tool workflow is illustrated in Figure 1.3.

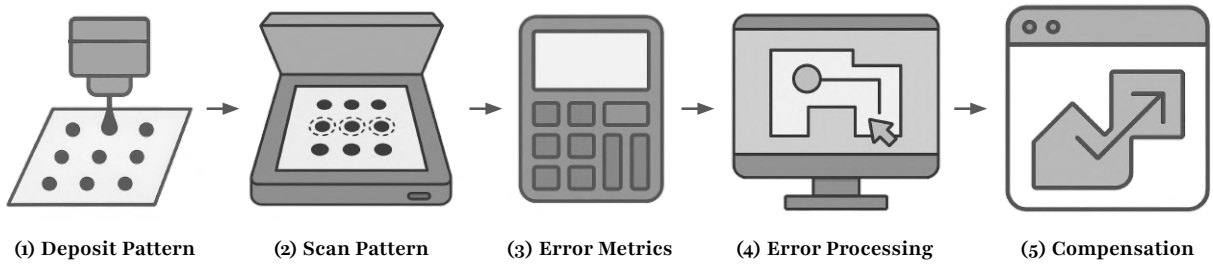

Figure 1.3: Scanner-based diagnostic pipeline for evaluating jetting fidelity and dopant distribution in RFAM. (1) A controlled droplet pattern is deposited. (2) The printed substrate is scanned using a high-resolution flatbed scanner. (3) Quantitative error metrics, such as centroid deviation and halo eccentricity, are extracted from the image. (4) These metrics are processed to identify geometric and material deviations. (5) Compensation is applied to the input toolpaths to improve future print accuracy.

1.2.1 Motivation and Background

Flatbed scanners have been extensively validated for print quality assessment due to their high spatial resolution, radiometric consistency, and low cost [33, 38]. These same traits make them an ideal tool for ex-situ analysis in additive manufacturing. Scanner-based image analysis has been successfully applied to printed electronics, colorimetric sensors, and microfluidic platforms [35–37].

Commercial tools like JetXpert and high-speed cameras are powerful but cost-prohibitive and limited to specialized labs. This scanner-based method offers comparable insights using widely accessible tools and open-source software, enabling broader adoption and iteration during RFAM process development.

1.2.2 Method Overview

The diagnostic process begins with substrate selection. Chromatography or blotting paper is used for dopant concentration analysis due to its ability to absorb and spread droplets into consistent, analyzable halos [35–37]. For spatial placement analysis, low-wicking substrates are used to limit fluid spread and preserve precise droplet locations.

Patterns are imaged using a flatbed scanner with a minimum resolution of 4800 dpi (5.29 μm pixel pitch), which ensures high spatial fidelity under diffuse, uniform illumination. A NIST-traceable calibration ruler is scanned to provide dimensional scaling [33, 38].

Printed test patterns consist of droplet grids with controlled drop count and spacing to assess spatial accuracy and material deposition repeatability [33, 34]. For dopant concentration analysis, droplets of known volume are deposited and later analyzed based on grayscale intensity (Figure 1.4). Prior studies have shown that classical image features such as centroid deviation and eccentricity provide accurate, image-only diagnostics of jetting fidelity [34, 39].

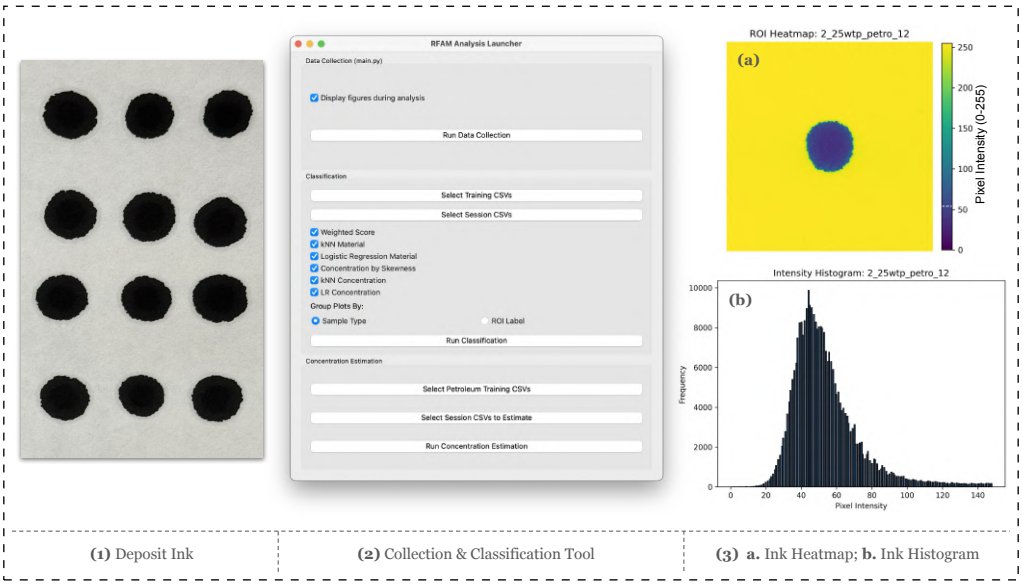

Figure 1.4: Example of ink analysis tool: (1) deposit ink, (2) classify samples using training data, (3) generate outputs such as (a) heatmaps and (b) histograms for concentration analysis.

1.2.3 Image Processing and Analysis Pipeline

Captured images are analyzed using custom Python and OpenCV scripts to extract quantitative metrics from each printed test pattern. First, (1) droplet centroids are located and compared against nominal grid targets to compute positional deviations and assess spatial accuracy. Next, (2) halo shape, area, and eccentricity are measured to evaluate nozzle alignment and infer relative droplet volume. Finally, (3) grayscale intensity values are sampled from doped regions and mapped to dopant concentration using calibration curves developed from manual ink deposition of known volumes and carbon content. The resulting data are used to quantify placement error, material distribution, and confirm spatial carbon content.

In addition to paper substrate-based tests, the diagnostic pipeline must also be validated at the part scale to confirm tool performance. Green-state components are printed and analyzed

using X-ray computed tomography (CT) to measure bulk dimensional accuracy. Differences between natural nylon and doped nylon regions are quantified, and reconstructed geometries are compared against both CAD models and input toolpaths. This complementary analysis verifies that scanner-based measurements correlate with actual part fidelity, extending the diagnostic method from droplet-level assessments to full 3D structures and demonstrating applicability to substrate mediums such as nylon powder beds.

1.2.4 Error Characterization and Process Feedback

The ex-situ diagnostic pipeline provides image-based metrics, including centroid deviation, halo eccentricity, and grayscale intensity, that map directly to RFAM error sources. These enable systematic correlations between observed defects and mechanical or process irregularities. Global offsets often indicate gantry misalignment, backlash, or toolpath scaling errors. Halo eccentricity reflects nozzle angle deviation or jetting asymmetry. Grayscale intensity variations signal dopant concentration inconsistencies due to ink pressure or printhead instability.

These metrics inform practical correction strategies. For example, repeated scans of a 25 mm square target showing a consistent +0.1 mm oversize in X lead to a 0.996 scale factor applied in software. Halo shape metrics guide nozzle alignment, while grayscale analysis supports ink delivery tuning. Though not yet real-time, the framework lays the foundation for in-situ correction. Combined with modeling from Task 2, this strategy enables calibration and refinement, improving part quality without costly in-situ hardware.

1.3 Expected Contributions

This task introduces innovations in both machine architecture and process diagnostics that enable reproducible, high-fidelity Radio Frequency Additive Manufacturing (RFAM). The key contributions are as follows:

- **Design of a Modular RFAM Platform:** A custom-built, binderjet-style RFAM system is developed to support volumetric sintering via dopant patterning and targeted RF exposure. The platform integrates high-resolution motion control, interchangeable material handling units, and modular gantries for printing and recoating. Critically, it includes a purpose-designed Faraday cage and RF delivery system operating at 13.56 MHz, enabling full-field volumetric energy delivery experiments.
- **Low-Cost, High-Resolution Diagnostic Pipeline:** This work introduces a novel ex-situ diagnostic tool that combines flatbed scanner imaging with open-source image analysis to assess jetting fidelity, dopant distribution, and concentration. In addition to paper-based tests, the pipeline is validated at the part scale using X-ray computed tomography (CT) of green-state components to quantify dimensional accuracy and compare reconstructed geometries against CAD and toolpaths. Together, these approaches provide a quantitative, repeatable, and cost-effective alternative to high-speed camera systems or in-situ metrology, democratizing access to print quality diagnostics in AM research environments.

Together, these contributions establish a flexible and scalable RFAM research platform that integrates accessible diagnostics with precision machine control. This foundation supports future correction strategies and closed-loop control for volumetric additive manufacturing.

Task 2: Toward Ideal Parts and Geometric Precision via Computational Solutions

Having established a custom machine platform capable of precise dopant deposition and RF energy delivery, attention now shifts to the process-level challenges unique to Radio Frequency Additive Manufacturing (RFAM). Unlike surface-scanning methods such as Selective Laser Sintering (SLS), RFAM introduces energy volumetrically, allowing entire regions of a part to sinter simultaneously. This enables potential improvements in throughput and energy efficiency but also introduces complex interactions between geometry, heat, and material flow [29, 30, 40, 41].

This task explores advanced computational methods and multiphysics finite element analysis (FEA) to simulate the RF heating process. The framework models the coupled effects of electromagnetic fields, thermal diffusion, and sintering kinetics using COMSOL Multiphysics [28, 42–44]. Computational strategies such as functional grading, input image pre-distortion (pre-warping), and field averaging are investigated to improve spatial control of energy absorption [45]. Insights from these simulations are used to optimize dopant distributions and energy delivery strategies.

2.1 Key Challenges in the RFAM Process

Radio Frequency Additive Manufacturing (RFAM) introduces energy volumetrically through RF heating, enabling high-throughput sintering of polymer powders doped with susceptor materials such as graphite or carbon black. However, this approach departs fundamentally from surface-scanning sintering techniques and brings several critical challenges that must be resolved to achieve high-quality, geometrically accurate parts [29, 30].

To realize the potential of RFAM, several critical challenges must be addressed:

- **Volumetric Densification and Shrinkage:** One of the most significant challenges in RFAM is managing the extreme volumetric reduction that occurs during densification. As observed in Selective Laser Sintering of polyamide powders like PA12, the sintered region can reduce significantly in volume as the porous powder bed transitions to a fully dense solid. This shrinkage is a result of particle coalescence, pore collapse, and polymer chain entanglement under elevated temperature [29, 46–48]. In RFAM, this effect is compounded across hundreds or thousands of layers, risking internal porosity, interfacial delamination, and geometric drift over the full build height [29]. Unlike laser sintering, which fuses localized areas layer-by-layer with controlled melt pools and open surface convection, RFAM introduces energy volumetrically, creating additional challenges in synchronizing material flow and shrinkage. To counteract these effects, active compression strategies are being explored that can mechanically constrain or direct shrinkage during the sintering process, maintaining part integrity, surface fidelity, and dimensional accuracy.

- **Void Formation from Rapid Heating:** The rapid volumetric heating inherent to RF coupling can lead to void formation if dopant particles heat faster than the surrounding polymer can respond [29]. In addition to thermal mismatch, heating efficiency and spatial uniformity are strongly influenced by the dielectric properties of the doped

material. The ability of the material to absorb and dissipate RF energy depends not only on dopant concentration, but also on polymer matrix characteristics, dispersion uniformity, and frequency-dependent loss behavior [30]. To minimize rapid heating and promote greater field homogeneity, a frequency of 13.56 MHz is selected. Its longer wavelength produces lower energy density and more uniform wave propagation compared to 27.12 MHz RF or 2.45 GHz microwave systems [40, 41, 45]. In contrast to microwave heating, RF fields exhibit less constructive and destructive interference, thereby reducing the formation of hot and cold spots. At 13.56 MHz, the wavelength is approximately 22.11 m, compared to only 0.12 m at 2.45 GHz. This frequency therefore provides a balance between effective energy delivery and spatial uniformity, mitigating localized overheating and reducing the likelihood of void formation in RFAM.

- **Boundary Oversintering:** Unlike laser-based systems where energy is directly patterned, RFAM relies on spatially patterned dopants to localize heating. This indirect control of energy can lead to coalescence of undesired particles at feature boundaries, as heat spreads beyond the intended regions due to thermal diffusion [29]. To address this, binding ink materials that act as mechanical-thermal barriers are being investigated. These are analogous to detailing agents used in high-speed sintering. Additional approaches will be explored to improve edge definition and geometric precision.

- **Geometry-Dependent Heating Uniformity:** Achieving uniform heating across complex geometries is non-trivial; anisotropic heat accumulation arises from geometry-dependent field interactions (e.g., circular vs. square cross-sections). A turntable mechanism will be implemented to minimize directional bias in field exposure, and computationally generated functional grading maps will be used to compensate for predicted thermal gradients [30]. However, functional grading introduces a trade-off: excessive dopant modification can distort fine features or cause shape deviations, especially in sharp-edged or thin-walled regions [30]. These effects must be carefully balanced during computational optimization to preserve part accuracy while achieving desirable thermal performance.

- **RF Wave Interference in Multi-Part Builds:** In densely packed builds, dopant-rich regions can disrupt RF propagation, effectively shielding downstream features. Turntable rotation offers partial relief, but future work must develop spatial arrangement strategies to enable consistent sintering of multiple parts per layer [30].

These challenges are interdependent and often nonlinear in effect, requiring a simulation-based framework that captures the coupling between electrical, thermal, and material behaviors. The following sections outline how such a framework is constructed and leveraged to address these issues.

2.2 Simulation Framework for Achieving Thermal Uniformity in RFAM

Achieving uniform energy absorption during sintering is essential for producing dimensionally accurate and mechanically consistent parts in RFAM. Unlike surface-based systems that raster energy across the build plane, RFAM volumetrically deposits energy using alternating

electric fields at 13.56 MHz. As a result, thermal gradients emerge due to spatial variation in field strength, dopant distribution, part geometry, and boundary effects [30]. These nonuniformities lead to challenges such as oversintering, incomplete fusion, void formation, and edge distortion.

To address these phenomena and the process challenges laid out in Section 2.1, a multi-physics simulation framework is developed to model electromagnetic heating and transient thermal diffusion. This framework provides insight into energy deposition patterns and thermal response, enabling predictive design strategies to mitigate geometric distortion and improve part quality.

The modeling approach consists of two primary physics domains:

- **Electromagnetic Field Simulation:** A quasi-static electric currents model solves for the electric field distribution within the powder bed. This approach assumes dominant conduction losses in lossy materials, such as graphite-doped Nylon-12, and neglects displacement currents. Volumetric power dissipation is computed from the electric field using a Joule heating formulation.

- **Transient Heat Transfer:** The power dissipation field is passed to a time-dependent heat conduction model that captures temperature evolution during the RF heating cycle. Material-specific parameters, such as density, heat capacity, and thermal conductivity, are used to define the thermal response. Where available, temperature-dependent properties are incorporated to improve accuracy.

Simulation domains are defined by the CAD geometry of the green part and surrounding powder, with electrical conductivity interpolated from experimental measurements of doped powder blends. The conductivity field varies spatially according to dopant concentration derived from print data or design files.

Because full-wave EM solvers are computationally prohibitive at 13.56 MHz, this quasi-static formulation offers a practical balance of accuracy and efficiency. Though it does not fully capture wave reflections or interference effects, it is sufficient for estimating localized power deposition in conduction-dominated media [28, 42, 43].

The simulation outputs include:

- Spatial electric field intensity and power density, $Q(\mathbf{r})$, where $\mathbf{r} = (x, y, z)$ is the position vector in 3D space. This represents localized volumetric heating due to RF field coupling with conductive regions of the powder bed.

- Transient temperature fields, $T(\mathbf{r}, t)$, and gradients, ∇T, where t is the elapsed time during the RF heating cycle. These fields track how temperature evolves spatially and temporally throughout the part and surrounding powder.

- Peak temperatures and time histories at selected locations, which can be compared to IR camera data. Validation to be performed via IR camera measurements (FLIR A70).

These simulations reveal process-critical phenomena such as hotspots at sharp corners, voids in thick sections, and edge-driven thermal distortion. An example simulation result is shown in Figure 2.1, which highlights the pronounced heating near the square part's corners,

consistent with experimental observations [30]. Such insights inform strategies like functional grading, pre-warping of geometries, and turntable-based angular averaging, all of which are discussed in Section 2.3.

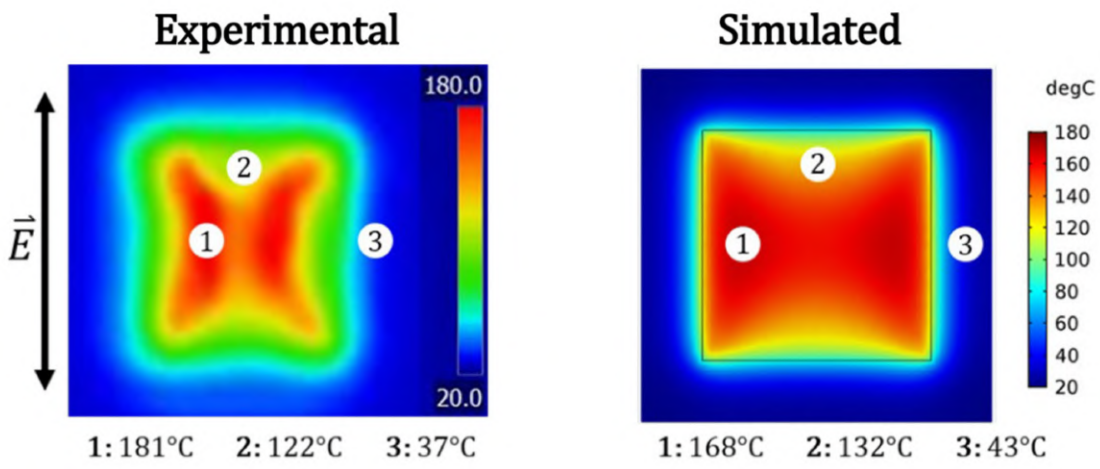

Figure 2.1: Simulation of RF heating distortion of a square cross-section [30].

2.3 Simulation-Informed Strategies for Process Compensation

Simulation results highlight the key thermal and geometric challenges of RFAM: localized under/overheating, void formation, part shrinkage, and angular field nonuniformity. To address these, computational outputs are used to guide several corrective strategies that modulate energy input, compensate for heat-driven distortion, and homogenize field exposure.

2.3.1 Functional Grading of Dopant Concentration

Functional grading adjusts the local electrical conductivity of the powder bed by varying dopant concentration. Because volumetric power dissipation scales with conductivity and electric field intensity, spatial tuning of dopant distribution can suppress overheating in high-field regions and boost energy input in underexposed zones [28, 44].

Simulation-driven power maps are used to define doping profiles, where regions with excess heating receive lower dopant loading. These corrections are implemented at the droplet scale, capable of depositing ink with dopant concentrations up to 25 wt%. This resolution exceeds prior work and enables targeted shaping of power density fields within complex part geometries.

2.3.2 Input Image Pre-Distortion

Geometric distortion due to non-uniform heating, differential thermal expansion, and shrinkage can be predicted by evaluating spatial temperature gradients from the thermal model. These gradients induce warping, especially at free edges and unsupported overhangs.

By simulating the expected thermal profile and shrinkage behavior, geometric compensation can be applied upstream by pre-warping the input CAD model. This forward design approach allows the final sintered geometry to contract into the desired form. A parallel exists in semiconductor manufacturing through Inverse Lithography Technology (ILT), a

model-based computational method used to generate photomasks that account for optical distortion and process variability in sub-wavelength lithography [49–51]. ILT solves the inverse imaging problem by determining an input mask pattern that produces the desired printed features after all system-level distortions are applied (Figure 2.2).

In RFAM, a similar computational inversion strategy can be applied: the input dopant pattern is optimized to yield a target post-sintering geometry. By incorporating thermal simulation outputs into the pre-warping algorithm, the process enables higher geometric fidelity and aligns with broader goals of closed-loop, model-informed additive manufacturing. Several ILT variants, including graph-based and learning-accelerated methods, offer promising pathways for fast, convergent optimization of input fields in this context [52, 53].

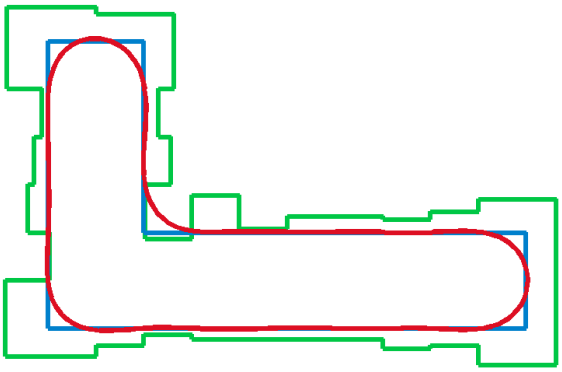

Figure 2.2: An illustration of Inverse Lithography Technology (ILT). The blue Γ-like shape represents the desired feature. The green shape shows the optimized photomask produced through inverse lithographic computation. The red contour indicates the actual printed result on the wafer [54].

2.3.3 Turntable-Based Field Averaging

Electric field strength is sensitive to part orientation relative to the electrodes, leading to asymmetries in heating. To mitigate this, a rotating platform is introduced beneath the powder bed to time-average the angular exposure to the RF field. Simulations of stationary vs. rotating builds confirm that turntable motion smooths energy delivery, reducing field concentration near edges and enabling more uniform sintering [30].

2.3.4 Dopant Ink Design

Ink formulation plays a critical role in RFAM by directly controlling local electrical conductivity and, thus, energy absorption under RF exposure. Experimental characterization of graphite-doped nylon powder blends revealed that dopant concentrations between 25–35 wt% produce the most effective heating response at 27.12 MHz, as demonstrated in prior volumetric RFAM studies [29].

Building on this, high-performance jettable inks have been developed in collaboration with Nazdar, a commercial ink supplier, achieving graphite loadings up to 25 wt% while maintaining viscosity and stability suitable for industrial inkjet systems.

2.4 Expected Contributions

This task presents several contributions that advance the precision, repeatability, and thermal control of RFAM through computational and process development:

- **High-Resolution Functional Grading:** Building on prior low-resolution approaches [30], this work introduces droplet-scale spatial control over dopant concentration to modulate local power density. This enables refined energy shaping across complex geometries, enhancing thermal uniformity without compromising feature fidelity.
- **Geometric Pre-Warping:** A model-informed design strategy inspired by Inverse Lithography Technology (ILT) is applied to compensate for thermal distortions. Input geometries are pre-distorted based on electromagnetic thermal simulation outputs, allowing the final sintered part to conform to the intended shape.
- **Rotational Field Averaging:** A turntable-based mechanism is introduced to average directional RF field exposure over time, mitigating angular heating asymmetries and promoting more uniform sintering.
- **Jettable Inks with High Dopant Loadings:** Inks with up to 25 wt% graphite have been developed in collaboration with Nazdar, enabling stable jetting while maintaining the high loss tangents required for RF heating. These inks support high-resolution functional grading and expand the processable material space in RFAM.

Task 3: Expanding Radio Frequency Applications in Additive Manufacturing: New Materials and Process Modalities

While previous tasks have focused on refining Radio Frequency Additive Manufacturing (RFAM) through geometric compensation, thermal simulation, and diagnostic feedback, the long-term utility of RFAM also depends on its adaptability across material systems and process architectures. Unlike conventional heat sources in additive manufacturing, such as lasers, RF energy can activate materials volumetrically and selectively based on their electromagnetic properties, opening new pathways for energy-directed fabrication. This task explores new process modalities that extend RFAM beyond carbon-doped nylon powder beds.

3.1 Criteria for RF-Responsive Materials

Expanding the RFAM process into new domains requires identifying materials that effectively couple with RF energy and are compatible with additive workflows. Suitable candidates typically exhibit high dielectric or conductive losses to ensure efficient RF energy absorption [43, 55]. Depending on the specific process modality, such as suspended extrusion or foam expansion, materials must also display appropriate rheological properties to support flow and shape retention. These criteria collectively inform material selection across the RFAM modalities introduced in the sections that follow.

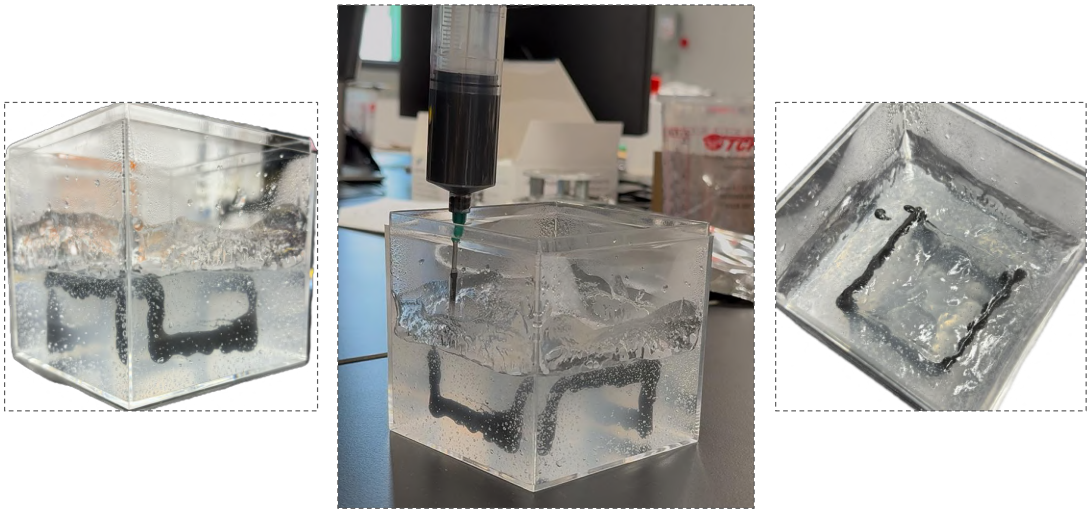

Figure 3.1: Sample of bath printing with graphite-doped silicone in hydrogel bath.

3.2 Volumetric RF Curing of Doped Silicone in Viscous Baths

This modality of RFAM explores the extrusion of graphite-doped silicones into a viscous, RF-transparent bath that enables suspended part formation and eventually, in-situ volumetric curing (as illustrated in Figure 3.1). As the doped material is deposited, it remains stationary within the bath medium and undergoes localized heating upon exposure to an RF field applied between surrounding electrodes. Dielectric and conductive losses within the doped polymer result in internal heating and crosslinking, enabling structurally stable features to form without the need for external curing or sacrificial supports.

Successful implementation of this process requires careful design of both the ink and bath. The silicone must incorporate uniformly dispersed conductive fillers, such as graphite or carbon black, to ensure even heating while maintaining manageable viscosity and print resolution. Meanwhile, the support bath, typically composed of PEG-based fluids, silicone oils, or fluorinated oils, must remain transparent to RF radiation, suspend the printed silicone without inducing flow, and avoid inhibiting silicone crosslinking.

This architecture enables the fabrication of overhanging, freeform, and lattice-like structures in elastomeric materials. Overall, this process showcases the flexibility of RF energy as both an activation and fabrication mechanism within soft matter additive manufacturing.

3.3 RF-Induced Expansion of Open-Cell Silicone Foams

This modality uses RF energy to simultaneously cure and expand graphite-doped silicone into lightweight, open-cell foams (Figure 3.2). Thermally activated, gas-releasing additives, such as *p-toluenesulfonyl hydrazide (TSH)*, are blended into the matrix. Upon RF exposure, volumetric heating initiates both polymer crosslinking and nitrogen gas release, forming porous elastomeric structures without molds, ovens, or tooling. RF's temporal tunability enables precise control over foam morphology and mechanical response.

Material compatibility is key: platinum-catalyzed silicones are inhibited by water, requiring anhydrous foaming agents. TSH decomposes near 130 °C to 140 °C, releasing N_2 without water [56, 57]. It is widely used in thermoplastics and elastomers as a fine powder suitable for silicone dispersions. Conductive dopants such as graphite or carbon black must be uniformly dispersed to ensure homogeneous RF heating and avoid local over-curing.

Applications include soft padding and energy-absorbing components where traditional foaming methods are impractical. This process highlights RFAM's ability to spatially and selectively activate soft, reactive materials.

(a) (b) (c)

Figure 3.2: Silicone foam expansion tests evaluating minimum mold volume required for RF-induced curing. Samples correspond to identical projected areas (637.4 mm^2) with mold depths of **(a)** 2 mm (1274.9 mm^3), **(b)** 3 mm (1912.3 mm^3), and **(c)** 5 mm (3187.2 mm^3).

3.4 Selective RF Actuation for Programmable Deformation

Radio frequency fields can serve not only as fabrication energy sources but also as stimuli for post-process actuation. By spatially patterning conductive dopants within a printed structure, it is possible to concentrate heating effects in targeted regions upon RF exposure.

The resulting localized thermal gradients drive deformation in thermally responsive matrices, enabling programmable motion without embedded electronics or tethered power.

Dopant patterning is central to this approach. Conductive fillers such as graphite or carbon black may be selectively deposited during fabrication through ink jetting, or applied post-process via painting, spraying, or screen printing. These doped regions couple with the RF field to produce localized heating, while undoped regions remain unaffected. The host material, typically an elastomer like PDMS, must exhibit thermal responsiveness such as softening, swelling, or phase change at the induced temperatures. This enables controlled bending, twisting, or expansion in specific areas of the part.

Exposure duration and field strength govern activation magnitude, and fabrication methods range from direct dopant deposition to hybrid assembly of doped and undoped components. Potential applications include soft robotic grippers with doped hinge zones that curl in response to RF exposure, deployable structures that change shape on demand, and wearable devices capable of localized compression or airflow control. While these deformations do not impart force unless coupled with stored mechanical energy, they enable programmable, material-driven shape change without embedded electronics. These examples show how RF heating can be used to embed shape-changing functionality directly into fabricated parts without added hardware.

3.5 Expected Contributions

This task introduces three new process modalities that extend the utility of Radio Frequency Additive Manufacturing (RFAM) beyond traditional powder bed systems. Each modality leverages RF energy's volumetric and selective heating characteristics to enable material–process combinations that are difficult or infeasible with conventional laser-based techniques:

- **Volumetric RF Curing in Viscous Baths:** A new fabrication architecture in which doped silicone is extruded into an RF-transparent, viscous bath and cured volumetrically in situ. This enables suspended, support-free formation of elastomeric geometries including overhangs and lattice structures.
- **RF-Induced Foam Expansion:** Silicone composites with gas-releasing additives are simultaneously cured and expanded using RF energy. The result is lightweight, open-cell foams formed without molds or ovens, with tunable porosity controlled via formulation and exposure parameters.
- **Selective RF-Induced Deformation via Embedded Dopants:** Spatially patterned conductive fillers enable localized RF heating and material-driven shape change in thermally responsive elastomers, supporting untethered reconfiguration without embedded electronics or actuators.

Collectively, these modalities show that RF energy, previously limited to niche heating applications, can now be harnessed to fabricate, shape, and program materials within a broad additive manufacturing toolkit.

Timeline for Proposed Work

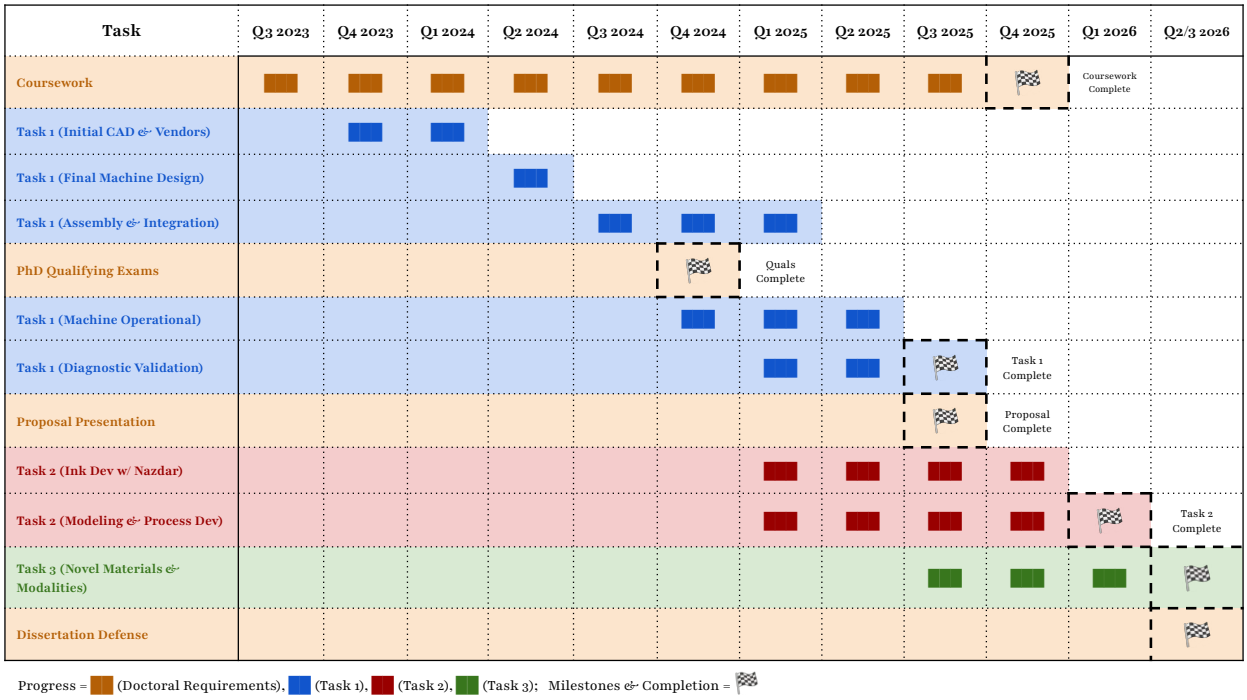

Figure 4.1: Ph.D. dissertation timeline and milestone chart (August 2023 – September 2026).

References

[1] I. Gibson, D. Rosen, and B. Stucker. *Additive Manufacturing Technologies: 3D Printing, Rapid Prototyping, and Direct Digital Manufacturing*. Springer, 2015. DOI: 10.1007/978-1-4939-2113-3.

[2] J. J. Beaman, D. L. Bourell, C. C. Seepersad, and D. Kovar. "Additive manufacturing review: early past to current practice". In: *Journal of Manufacturing Science and Engineering* (2020). DOI: 10.1115/1.4048193. URL: https://asmedigitalcollection.asme.org/manufacturingscience/article-abstract/142/11/110812/1086507.

[3] S. Yang and Y. Zhao. "Additive manufacturing-enabled design theory and methodology: a critical review". In: *International Journal of Advanced Manufacturing Technology* (2015). DOI: 10.1007/s00170-015-6994-5. URL: https://link.springer.com/article/10.1007/s00170-015-6994-5.

[4] X. Yao, S. Moon, and G. Bi. "A Cost-Driven Design Methodology for Additive Manufactured Variable Platforms in Product Families". In: *J. Mech. Des.* 138.4 (2016), p. 041701. DOI: 10.1115/1.4032504.

[5] P. Charalampous, I. Kostavelis, and D. Tzovaras. "Non-destructive quality control methods in additive manufacturing: A survey". In: *Rapid Prototyp. J.* 26.5 (2020), pp. 777–790. DOI: 10.1108/rpj-08-2019-0224.

[6] T. DebRoy, W. Zhang, J. Turner, and S. Babu. "Building digital twins of 3D printing machines". In: *Scr. Mater.* 135 (2017), pp. 119–124. DOI: 10.1016/j.scriptamat.2016.12.005.

[7] L. Bahruni, M. Rivette, A. Rechia, A. Siadat, and A. Elmesbahi. "Additive manufacturing technology: The status, applications, and prospects". In: *Int. J. Adv. Manuf. Technol.* 97 (2018), pp. 147–161. DOI: 10.1007/s00170-018-1932-y.

[8] H. Ko, S. Moon, and J. Hwang. "Design for additive manufacturing in customized products". In: *Int. J. Precis. Eng. Manuf.* 16 (2015), pp. 2369–2375. DOI: 10.1007/s12541-015-0305-9.

[9] C. R. Deckard. "Method and apparatus for producing parts by selective sintering". Patent US4863538A. 1989. URL: https://patents.google.com/patent/US4863538A/en.

[10] D. L. Bourell, T. J. Watt, D. K. Leigh, and B. A. Fulcher. "Performance limitations in polymer laser sintering". In: *Physics Procedia* 56 (2014), pp. 147–156. DOI: 10.1016/j.phpro.2014.08.157.

[11] A. Jabri, A. Layadi, and A. Benamrouche. "A comprehensive review of polymer materials and selective laser sintering technology for 3D printing". In: *Mechanik* 96.9 (2023), pp. 5–17. DOI: 10.5604/01.3001.0053.7286.

[12] P. Peyre, Y. Rouchausse, D. Defauchy, and G. Régnier. "Experimental and numerical analysis of the selective laser sintering (SLS) of PA12 and PEKK semi-crystalline polymers". In: *Journal of Materials Processing Technology* 225 (2015), pp. 326–336. ISSN: 0924-0136. DOI: 10.1016/j.jmatprotec.2015.04.030. URL: https://www.sciencedirect.com/science/article/pii/S092401361500196X.

[13] L. Verbelen, S. Dadbakhsh, M. Van den Eynde, J.-P. Kruth, B. Goderis, and P. Van Puyvelde. "Characterization of polyamide powders for determination of laser sintering processability". In: *European Polymer Journal* 75 (2016), pp. 163–174. DOI: 10.1016/j.eurpolymj.2015.12.014.

[14] M. Zhao, K. Wudy, and D. Drummer. "Crystallization Kinetics of Polyamide 12 during Selective Laser Sintering". In: *Polymers* 10.2 (2018), p. 168. DOI: 10.3390/polym10020168.

[15] D. T. Pham, K. D. Dotchev, and W. A. Y. Yusoff. "Deterioration of polyamide powder properties in the laser sintering process". In: *Proceedings of the Institution of Mechanical Engineers, Part C: Journal of Mechanical Engineering Science* 222.11 (2008), pp. 2163–2176. ISSN: 0954-4062. DOI: 10.1243/09544062JMES839. URL: https://doi.org/10.1243/09544062JMES839.

[16] J. Choren, V. Gervasi, T. Herman, S. Kamara, and J. Mitchell. "SLS Powder Life Study". In: *Proceedings of the 2001 International Solid Freeform Fabrication Symposium*. Available online: http://dx.doi.org/10.26153/tsw/3234. University of Texas at Austin, 2001. URL: https://hdl.handle.net/2152/76145.

[17] T. Gornet, K. Davis, T. Starr, and K. Mulloy. "Characterization of Selective Laser Sintering™ Materials to Determine Process Stability". In: *Proceedings of the 2002 International Solid Freeform Fabrication Symposium*. Available online: http://dx.doi.org/10.26153/tsw/4531. University of Texas at Austin, 2002. URL: https://hdl.handle.net/2152/77442.

[18] H. Zarringhalam, N. Hopkinson, N. Kamperman, and J. de Vlieger. "Effects of processing on microstructure and properties of SLS Nylon 12". In: *Materials Science and Engineering: A* 435–436 (2006), pp. 172–180. ISSN: 0921-5093. DOI: 10.1016/j.msea.2006.07.084. URL: https://www.sciencedirect.com/science/article/pii/S092150930601478X.

[19] S. Affolter, A. Ritter, and M. Schmid. "Interlaboratory Tests on Polymers by Differential Scanning Calorimetry (DSC): Determination of Glass Transition Temperature (T_g)". In: *Macromolecular Materials and Engineering* 286.10 (2001), pp. 605–610. ISSN: 1438-7492. DOI: 10.1002/1439-2054(20011001)286:10<605::AID-MAME605>3.0.CO;2-Y. URL: https://doi.org/10.1002/1439-2054(20011001)286:10%3C605::AID-MAME605%3E3.0.CO;2-Y.

[20] D. Bourell and J. Beaman Jr. "Materials Issues in Rapid Prototyping". In: *Virtual Modelling and Rapid Manufacturing: Advanced Research in Virtual and Rapid Prototyping*. Taylor & Francis Group, 2005, pp. 305–310.

[21] B. Xiao and Z. Ye. "Selective Laser Sintering: Processing, Materials, Challenges, Applications, and Emerging Trends". In: *Journal of Advanced Thermal Science Research* 11 (2024), pp. 65–99. DOI: 10.15377/2409-5826.2024.11.4.

[22] C. Deckard and D. Miller. "Improved Energy Delivery for Selective Laser Sintering". In: *Proceedings of the 1995 International Solid Freeform Fabrication Symposium*. Austin, TX: University of Texas at Austin, 1995. DOI: 10.15781/T26W96V1G. URL: http://hdl.handle.net/2152/68722.

[23] C. Lindemann, U. Jahnke, M. Moi, and R. Koch. "Analyzing Product Lifecycle Costs for a Better Understanding of Cost Drivers in Additive Manufacturing". In: *Proceedings of the 2012 International Solid Freeform Fabrication Symposium*. The University of Texas at Austin. Austin, TX: University of Texas at Austin, 2012. DOI: 10.26153/tsw/15341. URL: https://hdl.handle.net/2152/88402.

[24] L. Rickenbacher, A. Spierings, and K. Wegener. "An Integrated Cost-Model for Selective Laser Melting (SLM)". In: *Rapid Prototyping Journal* 19.3 (2013), pp. 208–214. DOI: 10.1108/13552541311312201.

[25] S. H. Khajavi, J. Partanen, and J. Holmström. "Additive Manufacturing in the Spare Parts Supply Chain". In: *Computers in Industry* 65.1 (2014), pp. 50–63. DOI: 10.1016/j.compind.2013.07.008.

[26] M. Barclift, S. Joshi, T. Simpson, and C. Dickman. "Cost Modeling and Depreciation for Reused Powder Feedstocks in Powder Bed Fusion Additive Manufacturing". In: *Proceedings of the 27th Annual International Solid Freeform Fabrication Symposium – An Additive Manufacturing Conference*. The University of Texas at Austin. Austin, TX, 2016. URL: https://repositories.lib.utexas.edu/server/api/core/bitstreams/c2115481-a9ed-4649-8239-8340e5d73c29/content.

[27] M. Baumers, C. Tuck, R. Wildman, I. Ashcroft, and R. Hague. "Energy Inputs to Additive Manufacturing: Does Capacity Utilization Matter?" In: *Proceedings of the 2011 International Solid Freeform Fabrication Symposium*. The University of Texas at Austin. Austin, TX: University of Texas at Austin, 2011. DOI: 10.26153/tsw/15275. URL: https://hdl.handle.net/2152/88336.

[28] J. Allison. "Radio Frequency Additive Manufacturing: A Volumetric Approach to Polymer Powder Bed Fusion". PhD thesis. The University of Texas at Austin, 2020.

[29] J. Allison, J. Pearce, J. Beaman, and C. Seepersad. "Volumetric fusion of graphite-doped nylon 12 powder with radio frequency radiation". In: *Rapid Prototyping Journal* 28.2 (2022), pp. 317–329. ISSN: 1355-2546. DOI: 10.1108/RPJ-09-2020-0218.

[30] J. Allison, J. Pearce, J. Beaman, and C. Seepersad. "Computational design strategy to improve RF heating uniformity". In: *Rapid Prototyping Journal* 28.8 (2022). Article published online: 8 March 2022; Issue publication date: 2 August 2022, pp. 1476–1491. ISSN: 1355-2546. DOI: 10.1108/RPJ-08-2021-0193.

[31] K. Wudy, D. Drummer, F. Kühnlein, and M. Drexler. "Selective Laser Sintering of Filled Polymer Systems: Bulk Properties and Laser Beam Material Interaction". In: *Physics Procedia* 83 (2016), pp. 991–1002. DOI: 10.1016/j.phpro.2016.08.104.

[32] Xaar. *Xaar Aquinox Printhead Technical Datasheet*. 2024.

[33] B. Streckel, B. Steuernagel, E. Falkenhagen, and E. Jung. "Objective Print Quality Measurements Using a Scanner and a Digital Camera". In: *IS&T's International Conference on Digital Production Printing and Industrial Applications (DPP)*. 2003, pp. 145–152. URL: https://www.academia.edu/10085543/Objective_Print_Quality_Measurements_Using_a_Scanner_and_a_Digital_Camera.

[34] M. Polomoshnov, K.-M. Reichert, L. Rettenberger, M. Ungerer, G. Hernandez-Sosa, U. Gengenbach, and M. Reischl. "Image-based identification of optical quality and functional properties in inkjet-printed electronics using machine learning". In: *Journal of Intelligent Manufacturing* 36 (2025), pp. 2709–2726. DOI: 10.1007/s10845-024-02385-4.

[35] Y. Soda and E. Bakker. "Quantification of Colorimetric Data for Paper-Based Analytical Devices". In: *ACS Sensors* 4 (2019), pp. 3093–3101. DOI: 10.1021/acssensors.9b01802.

[36] H. Shibata, Y. Hiruta, and D. Citterio. "Fully inkjet-printed distance-based paper microfluidic devices for colorimetric calcium determination using ion-selective optodes". In: *Analyst* 144 (2019), pp. 1178–1186. DOI: 10.1039/c8an02146e.

[37] Monisha, K. Shrivas, T. Kant, S. Patel, R. Devi, N. S. Dahariya, S. Pervez, M. K. Deb, M. K. Rai, and J. Rai. "Inkjet-printed paper-based colorimetric sensor coupled with smartphone for determination of mercury (Hg2+)". In: *Journal of Hazardous Materials* 414 (2021), p. 125440. DOI: 10.1016/j.jhazmat.2021.125440.

[38] K. Oskolok, E. Shults, O. Monogarova, and A. Chaplenko. "Optical molecular analysis using office flatbed photo scanner: New approaches and solutions". In: *Talanta* 178 (2018), pp. 377–383. DOI: 10.1016/j.talanta.2017.09.049.

[39] T. H. Phung, S. H. Park, I. Kim, T.-M. Lee, and K.-S. Kwon. "Machine learning approach to monitor inkjet jetting status based on the piezo self-sensing". In: *Scientific Reports* 13 (2023), p. 18089. DOI: 10.1038/s41598-023-45445-0. URL: https://www.nature.com/articles/s41598-023-45445-0.

[40] M. S. Ferdous, E. H. Koupaie, C. Eskicioglu, and T. Johnson. "An Experimental 13.56 MHz Radio Frequency Heating System for Efficient Thermal Pretreatment of Wastewater Sludge". In: *Progress In Electromagnetics Research B* 79 (2017), pp. 83–101. DOI: 10.2528/PIERB17091409.

[41] F. C. R. Wroe and A. T. Rowley. "Radio-frequency and microwave-assisted processing of materials". Patent CA2261995C (Canada). Granted September 28, 2004. Application originally filed by C Tech Innovation Ltd on July 24, 1997. 1998. URL: https://patents.google.com/patent/CA2261995C/en.

[42] K. W. K. Leung, A. Keshtgar, and N. Iyyer. "Heat Transfer Simulation for Reliability Estimation of Additive Manufacturing Process Using the COMSOL Multiphysics Software". In: *COMSOL Conference Proceedings*. 2017. URL: https://www.comsol.com/paper/heat-transfer-simulation-for-reliability-estimation-of-additive-manufacturing-process-using-the-comsol-multiphysics-software-37142 (visited on 03/11/2024).

[43] G. Li and J. Zhou. "COMSOL-Based Simulation of Microwave Heating of Al2O3/SiC Composites with Parameter Variations". In: *Symmetry* (2024). URL: https://www.mdpi.com/2073-8994/16/10/1254 (visited on 06/05/2025).

[44] Z. Chen. "Optimal Grading for Strength and Functionality of Parts Made of Interpenetrating Polymer Networks: Load Capacity Enhancement". PhD thesis. University of Nebraska, 2020. URL: https://digitalcommons.unl.edu/context/mechengdiss/article/1107/viewcontent/ZhongDissertation.pdf (visited on 03/11/2024).

[45] J. Seo, G. Han, and H. Hwang. "Uniform temperature distribution in microwave heating achieved via rotating electric field". In: *Scientific Reports* 15 (2025), p. 17960. DOI: 10.1038/s41598-025-03373-1. URL: https://doi.org/10.1038/s41598-025-03373-1.

[46] A. Mokrane, M. Boutaous, and S. Xin. "Process of selective laser sintering of polymer powders: Modeling, simulation, and validation". In: *Comptes Rendus Mécanique* 346.12 (2018), pp. 1087–1103. DOI: 10.1016/j.crme.2018.08.002. URL: https://doi.org/10.1016/j.crme.2018.08.002.

[47] F. Lupone, E. Padovano, F. Casamento, and C. Badini. "Process Phenomena and Material Properties in Selective Laser Sintering of Polymers: A Review". In: *Materials* 15.1 (2021), p. 183. DOI: 10.3390/ma15010183.

[48] C. Meier, R. Weissbach, J. Weinberg, W. A. Wall, and A. J. Hart. "Critical Influences of Particle Size and Adhesion on the Powder Layer Uniformity in Metal Additive Manufacturing". In: *CoRR* abs/1804.06822 (2018). arXiv: 1804.06822. URL: http://arxiv.org/abs/1804.06822.

[49] A. Poonawala and P. Milanfar. "Mask design for optical microlithography—An inverse imaging problem". In: *IEEE Transactions on Image Processing* 16.3 (2007), pp. 774–788. DOI: 10.1109/TIP.2006.891332.

[50] L. Pang. "Inverse lithography technology: 30 years from concept to practical, full-chip reality". In: *Journal of Micro/Nanopatterning, Materials, and Metrology* 20.3 (2021), p. 030901. DOI: 10.1117/1.JMM.20.3.030901.

[51] S. H. Chan, A. K. Wong, and E. Y. Lam. "Initialization for robust inverse synthesis of phase-shifting masks in optical projection lithography". In: *Optics Express* 16.19 (2008), pp. 14746–14760. DOI: 10.1364/OE.16.014746.

[52] S. Zhang, X. Ma, and J. Zhang. "Fast inverse lithography approach based on a model-driven graph convolutional network". In: *Optics Express* 31.22 (2023), pp. 36451–36467. DOI: 10.1364/OE.493178.

[53] B. Zhu, S. Zheng, Z. Yu, G. Chen, Y. Ma, and F. Yang. "L2O-ILT: Learning to Optimize Inverse Lithography Techniques". In: *IEEE Transactions on Computer-Aided Design of Integrated Circuits and Systems* 43.3 (2024), pp. 944–955. DOI: 10.1109/TCAD.2023.3323164.

[54] Wikipedia contributors. *Inverse lithography — Wikipedia, The Free Encyclopedia*. https://en.wikipedia.org/wiki/Inverse_lithography. Accessed: 2025-07-22. 2024.

[55] N. Patil, A. C. Camacho, N. K. Mishra, P. Singhla, C. B. Sweeney, M. A. Saed, M. Radovic, and M. J. Green. "Radio Frequency and Microwave Heating of Preceramic Polymer Nanocomposites with Applications in Mold-Free Processing". In: *Advanced Engineering Materials* (2023). DOI: 10.1002/adem.201900276. (Visited on 06/05/2025).

[56] K. Li, M. Bai, J. Dang, et al. "Thermal hazard and decomposition mechanism of p-toluenesulfonyl hydrazide". In: *Journal of Thermal Analysis and Calorimetry* 149 (2024), pp. 6113–6124. DOI: 10.1007/s10973-024-13223-3. URL: https://doi.org/10.1007/s10973-024-13223-3.

[57] Wikipedia contributors. *p-Toluolsulfonsäurehydrazid — Wikipedia, die freie Enzyklopädie*. https://de.wikipedia.org/wiki/P-ToluolsulfonsÃd'urehydrazid. Translated from German to English. 2024. (Visited on 07/28/2025).